Journal of Computational Physics **162,** 82–103 (2000)
doi:10.1006/jcph.2000.6523, available online at http://www.idealibrary.com on IDEAL®

Low Frequency Finite Difference Time Domain (FDTD) for Modeling of Induced Fields in Humans Close to Line Sources

Michael E. Potter,* Michal Okoniewski,† and Maria A. Stuchly*

*Department of Electrical and Computer Engineering, University of Victoria, P.O. Box 3055 STN CSC, Victoria, British Columbia, Canada, V8W 3P6; and †Departement of Electrical and Computer Engineering, University of Calgary, 2500 University Drive, Calgary N.W., Alberta, Canada, T2N 1N4

Received August 10, 1999; revised April 6, 2000

The implementation of a low frequency line source as a source function in the finite difference time domain (FDTD) method is presented. The total–scattered field formulation is employed, along with a recently developed quasi-static formulation of the FDTD. Line-source modeling is important in the utility industry, where a more accurate prediction of the fields induced in workers in close proximity to power lines is required. The line-source representation is verified, and excellent agreement with analytic solutions is found for two object problems. A practical example of the electric fields and current densities induced in a human body in close proximity to a 60-Hz transmission line is evaluated. The results for predicted organ dosimetry for such a configuration are compared with predictions for the uniform electric field and demonstrate the induced fields and current densities can be significantly higher than originally predicted for the uniform electric field exposure on a ground plane.

Key Words: FDTD; quasi-static; power lines; induced fields; human body.

1. INTRODUCTION

The problem of human exposure to low frequency electromagnetic fields has been the subject of many studies and numerical simulations. The methods used for such numerical simulations range from integral equation (IE) methods, through finite difference (FD) techniques, to finite element methods (FEM). In all cases, advantage is taken of the quasi-static nature of the fields (and hence the quasi-static approximation to Maxwell's equations). IE methods are efficient for homogeneous shapes, but can require excessively large (possibly ill-conditioned) matrices when applied to large heterogeneous structures. FD methods are more flexible but can suffer from staircasing errors with the discretization

0021-9991/00 $35.00

of the object. Such staircasing errors can be effectively mitigated by the use of FEM because it lends itself well to adaptive mesh systems and mesh refinement. In general at low frequencies, Darwin approximations can be made [1] which provide elliptic equations from the modified Maxwell's equations, or Stevenson's method as outlined in [2] can be used.

In the case of high resolution numerical studies of the human body in the low-frequency field of a powerline, all three methods mentioned above produce enormous matrices to be solved. They are often not sparse because of the heterogeneity of the structure involved. Moreover, FD and FEM methods suffer from the lack of adequate free-space boundary conditions necessary to terminate the computational domain close to the body. As a result, the domain must be stretched to a distance of three times the body dimensions, thus increasing the volume by a factor of nine and further hampering the computational speed. The sheer size of the matrices makes it challenging at high resolution to avoid ill-conditioning.

In contrast, the finite difference time domain (FDTD), since its introduction by Yee [3], has been used extensively to model electromagnetic field interactions with complex heterogeneous structures. The FDTD technique has proven to be very flexible and effective in dealing with complex and dynamic problems, is easy to use, and is effective. It has become widespread and has been the subject of immense development over the past decades. A multitude of source functions for complex source geometries have also been successfully developed over the past 30 years. A major step forward in development of these source functions was the introduction of the total–scattered field formulation by Taflove [4]. This formulation allows for algorithms to efficiently implement uniform plane waves incident from arbitrary directions. This is particularly important for modeling problems where both the total and scattered fields are of interest.

In its classical form, the FDTD is not a very attractive method at low frequencies. The required simulation times may be prohibitively long even for moderate spatial resolution. However, at sufficiently low frequencies, and for suitable object dimensions and electrical properties, a recently proposed formulation [5] overcomes that problem. This formulation holds for quasi-static conditions, where the wavelength and skin depth are much greater than the size of the structure under consideration. It is also assumed that parts of the structure can be represented either as good conductors or as good dielectrics. The structure itself can be heterogeneous, but in any given part either the conduction or displacement current has to dominate to the extent that the other current component can be neglected (preferably it is below 0.1%). Under these conditions, the fields in the conductors are proportional to the time derivative of the incident field, and in dielectrics the induced fields follow the applied field temporal behavior. The field response needs to be computed separately for the electric and magnetic field. In practice, at low frequencies, the response to the electric or magnetic field alone is of interest anyway. By creating a standing wave condition, electric or magnetic field exposure can thus be studied in isolation.

For plane wave excitations with a ramp function, accurate results can be extracted immediately after the transient response has decayed, typically after 1000–4000 time steps [5] (i.e., a fraction of the signal period). A properly designed perfectly matched layer (PML) originated by Berenger [6] provides efficient low reflection termination of the computational space for this type of problem [7–9].

The quasi-static formulation of the FDTD was developed for evaluation of electric fields induced in the human body from exposure to powerline-frequency uniform electric fields.

The computations had to be performed with high resolution to identify organs that might have higher fields than the average. Thus the resolution used in the FDTD was 7.2 mm [5]. When the FDTD was hybridized with an efficient FD code, resolution of 3.6 mm was easily achieved with high accuracy [10]. This FD method was not hampered by the free space boundary conditions because the boundary condition was at the body surface and was simply the charge density developed by the exterior problem based on the lower resolution FDTD run. In some occupational situations, such as those in electric utility substations, workers on the ground are too close to the high voltage conductors for the exposure fields to be assumed to be uniform.

Although the total–scattered field formulation has so far been utilized for uniform plane wave excitation only, there is no reason why it cannot be extended to other excitations for which analytic solutions exist. We have previously demonstrated that we can implement the solution for an infinite line source at an arbitrary distance and orientation [11]. This modification to the FDTD program is important, since it allows for the prediction of fields and currents induced in utility workers in close proximity to powerlines. This in turn gives a more accurate picture of the hazards they are exposed to on a daily basis. The formulation of the line source in the FDTD may also be applied to other problems involving scattering from heterogeneous objects.

In this contribution the theory and implementation of the new line-source algorithm are outlined in detail, followed by a comprehensive verification. This includes comparisons with recently developed analytic solutions for a homogeneous lossy sphere in proximity of a current-carrying infinite conductor or an infinitely long uniform line of charge. The results referenced in [11] dealt specifically with the case of magnetic induction. Here we look at additional results for magnetic inductions and present results for electric induction. A discussion of staircasing errors and their impact are included, as well as methods of mitigating their effects. Finally, results are given for a high resolution heterogeneous model of the human body under a line source for electric field exposure (exposure to nonuniform magnetic fields can be efficiently evaluated by FD methods [12]).

2. THEORY

2.1. *Quasi-static FDTD Method*

Quasi-static approximations can be applied when the dimensions of the object of study are a fraction of a wavelength. Since using the quasi-static approximation implies that the electric and magnetic fields become decoupled, it is possible to study their effects in isolation. If one were to attempt to study extremely low frequency problems using the standard FDTD formulation, simulation times on the order of a few periods of the source would have to be used to reach steady state. For instance, for a problem at 60 Hz, with spatial discretizaton of $\Delta x = \Delta y = \Delta z = 0.5$ cm, from the Courant stability criterion, the duration of one time step would be $\Delta t = \Delta x/\sqrt{3}c = 9.6$ ps. Allowing for four periods of the source field, the number of time steps required for the simulation would be $N_{\Delta t} = 7 \times 10^9$. Even on a fast computer, the simulation would run for over one hundred years. For some simulations frequency scaling is used, but this approach has limitations—among them is that the fields are not decoupled. However, quasi-static approximations can be used to advantage in certain situations with the FDTD method, and thus the prohibitively long simulation time constraint is removed.

The quasi-static FDTD method as introduced in [5] is only briefly summarized here. The standard FDTD algorithm can be used to advantage with certain objects, since the phase relationships of fields in good conductors and dielectrics is known. Because conduction currents dominate displacement currents in conductors, and the opposite is true in dielectrics, the steady-state behaviour of fields can be predicted beforehand. Fields external to a conductor have the same phase as an incident field, whereas interior fields are first order in the quasi-static approximation and are therefore proportional to the time derivative of the incident field. By using a ramp function (which can be interpreted as an approximation to the start of a sinusoid), all fields in steady state attain either a linear (in good dielectrics) or a constant (in conductors) time behaviour after a short simulation time (a fraction of a period of the approximated sinusoid). To obtain a solution, it is therefore sufficient to obtain field values at two time steps after the transient response has decayed.

To reduce high-frequency contamination in simulations, a smoothed ramp function is used for the incident electric field E_{inc},

$$E_{\text{inc}} = \begin{cases} 0 & -\infty < t \leq t_0 \\ \cosh(t - t_0) - 1 & t_0 < t \leq \tau \\ A \times (t - \tau) + h & t > \tau, \end{cases} \tag{1}$$

where t is the time increment, t_0 is the starting point of the ramp (usually zero), and A is the desired slope of the ramp which is related to the peak amplitude and frequency of the sinusoid that is approximated. The constants τ and h are dependent on simulation parameters such as the grid and time discretization and serve to preserve continuity between the three sections of the ramp function.

In a standard FDTD program, the use of a single plane wave necessarily implies the fields are coupled. Quasi-static exposure can still be accomplished by creating a standing wave within the FDTD domain: exciting two plane waves in opposite directions using the total–scattered field formulation. By controlling the phase and amplitude, exposure either to only electric or magnetic fields can be created within a limited volume with dimensions much smaller than the wavelength.

In summary, the quasi-static FDTD method may be used when:

(i) in the object of study either the conduction or the displacement current dominates the other; and

(ii) the size of the object is much smaller than the incident field wavelength.

When these conditions are satisfied, electric or magnetic field exposure can be studied in isolation by creating an appropriate standing wave condition and by utilizing a ramp excitation function. It is important to note that the underlying FDTD method's numerical implementation (code) has not been modified: it is merely the utilization of a ramp function excitation and the creation of a standing wave that mimic quasi-static circumstances. The resultant fields must then be properly post-processed (i.e., scaling and/or differencing) to provide proper quasi-static results.

2.2. *Mathematical Basis of Transient Response*

From Maxwell's equations in the quasi-static limit it can be found that the time to steady state for electric or magnetic exposure is governed by relaxation or diffusion equations,

respectively. For each, there is a characteristic time constant which governs the transient response or, conversely, marks the transition to steady state. These time constants are $\tau_{\text{relaxation}} = \frac{\varepsilon}{\sigma}$ and $\tau_{\text{diffusion}} = \mu\sigma l^2$, where ε is the dielectric constant, σ is the conductivity, μ is the permeability, and l is the largest characteristic dimension of the object (i.e., diameter for a sphere). This in turn indicates when steady state is reached and when the simulation can be halted.

Although the exposure processes are governed by either relaxation or diffusion in real life, in the FDTD the coupling of the magnetic and electric fields cannot be separated to perfectly simulate a quasi-static situation. This can be accomplished indirectly by creating a standing wave, but both field vectors are still excited. For the case of a lossy object with conductivity, but relative permittivity and permeability of one, the diffusion time constant dominates. And so for both types of FDTD simulations (standing wave created for magnetic or electric exposure) the time to reach steady state is governed by the diffusion constant.

2.3. *Total–Scattered Field Formulation*

As outlined by Stratton [13],

> An electromagnetic field is uniquely determined within a bounded region V at all times $t > 0$ by the initial values of electric and magnetic vectors throughout V, and the values of the tangential component of the electric vector (or magnetic vector) over the boundaries for $t > 0$.

This provides the basis of the total–scattered field formulation introduced by Taflove [4]. In this formulation, splitting the computational domain into two regions separated by a Huygen's surface modifies the standard Yee algorithm [3]. Inside this closed surface the updated field values are still total fields, but outside the surface there are only scattered fields. By specifying the initial field values for the entire domain (usually zero), the tangential electric or magnetic field vectors at the Huygen's surface for all $t > 0$ can be specified, thus uniquely determining domain field values for all times $t > 0$.

The Huygen's surface field values can be decomposed into a scattered field component and an incident field component. The incident field values are derived from the source function. In the previously derived uniform plane wave source, the fields are uniquely specified by three fixed angles (ϕ, θ, ψ) which define the direction of propagation and the polarization of the electric field vector with respect to that direction. The angles ϕ and θ are the standard spherical coordinates (azimuth and elevation). The reference direction for ψ is the vector $\mathbf{k} \times \mathbf{z}$ where $\mathbf{k}$ is the incident wave vector direction, and ψ is measured clockwise (when looking towards the source) from the reference. This defines the electric field polarization on the transverse plane as illustrated in Fig. 1.

For the uniform plane wave formulation [4], a computationally efficient way to specify the incident wave components is through the use of an alternate one-dimensional source grid valid for propagation directions defined by the angles (ϕ, θ, ψ). Incident electric and magnetic field values on the Huygen's surface are then specified by interpolation of the field value in the source grid and implementation of appropriate connecting conditions. These connecting conditions are the Yee update equations, modified to incorporate an incident field component and a scattered field component.

The incident field vectors lie in planes transverse to the direction of propagation, at distances d along the source grid. Hence the incident fields must be transformed to Cartesian coordinates to be consistent with the Yee grid. The intersection of the Huygen's surface and these planes defines contours on which, for a uniform plane wave, all electric and magnetic

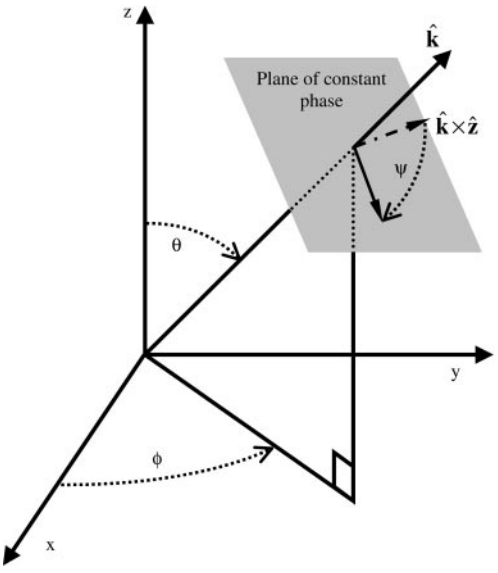

FIG. 1. Illustration of how the reference angles (ϕ, θ, ψ) are defined for an arbitrary incident wave vector **k**.

fields are identical. The appropriate equations for a uniform plane wave are [4]

$$H_{x,\mathrm{inc}}|_d^n = H_{\mathrm{inc}}|_d^n \times (\sin\psi \sin\phi + \cos\psi \cos\theta \cos\phi) \tag{2a}$$

$$H_{y,\mathrm{inc}}|_d^n = H_{\mathrm{inc}}|_d^n \times (-\sin\psi \cos\phi + \cos\psi \cos\theta \sin\phi) \tag{2b}$$

$$H_{z,\mathrm{inc}}|_d^n = H_{\mathrm{inc}}|_d^n \times (-\cos\psi \sin\theta) \tag{2c}$$

$$E_{x,\mathrm{inc}}|_d^n = E_{\mathrm{inc}}|_d^n \times (\cos\psi \sin\phi - \sin\psi \cos\theta \cos\phi) \tag{2d}$$

$$E_{y,\mathrm{inc}}|_d^n = E_{\mathrm{inc}}|_d^n \times (-\cos\psi \cos\phi - \sin\psi \cos\theta \sin\phi) \tag{2e}$$

$$E_{z,\mathrm{inc}}|_d^n = E_{\mathrm{inc}}|_d^n \times (\sin\psi \sin\theta), \tag{2f}$$

where $H_{\mathrm{inc}}|_d^n$ and $E_{\mathrm{inc}}|_d^n$ are the incident magnetic or electric field, respectively, at a distance d along the source grid and at time step n. For this uniform plane wave implementation the angles are fixed for all locations on the Huygen's surface.

2.4. *Line-Source Implementation*

The line-source implementation as reported in [11] is summarized here. For an infinite line of charge or current at a low frequency, the fields have a cylindrical TEM configuration. On a plane perpendicular to the line, the fields have magnitudes inversely proportional to the distance from the line and have a radial electric field and a circumferential magnetic field. These fields are thus transverse planar with their polarization dependent on their point in space with respect to the line. This immediately suggests how to modify Eqs. (2) to reflect this cylindrical TEM configuration. The source field values for the Huygen's surface are still transformed using (2), with the modification that the angle ψ is dependent on the distance vector **d** between that point in space and the line: $\psi = \psi(\mathbf{d})$. The TEM field **F**,

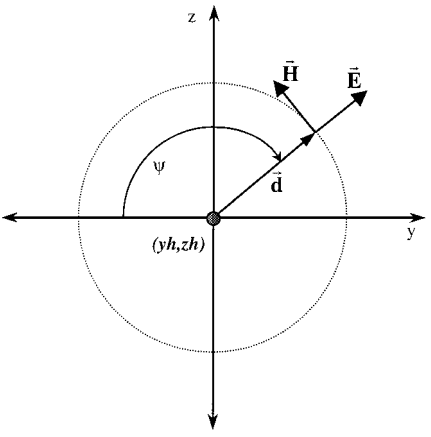

FIG. 2. Visualization for the angle ψ for a source wave (from a line source) in the $\hat{x}$ direction. Note the orientation of the vector couplet.

where **F** represents either the magnetic or electric field, can then be represented as:

$$\mathbf{F} = \frac{1}{|\mathbf{d}|}\mathbf{F}(\psi(\mathbf{d})). \tag{3}$$

Without loss of generality, it can be assumed that the infinite line source is oriented parallel to the x-axis and passes through the point (yh, zh). Then for any point on the Huygen's surface (x, y, z), to specify the incident field value, the scale factor is found as:

$$|\mathbf{d}| = \sqrt{(z - zh)^2 + (y - yh)^2}. \tag{4}$$

Also, to resolve the fields into three Cartesian components, Eqs. (2) still hold, with the modification that the angle ψ is

$$\psi(y, z; yh, zh) = \begin{cases} \arctan\left(\frac{z-zh}{y-yh}\right) & \mathbf{k} = -\hat{\mathrm{x}} \\ \arctan\left(\frac{z-zh}{yh-y}\right) & \mathbf{k} = +\hat{\mathrm{x}} \end{cases} \tag{5}$$

depending on the direction of the source wave. This is visualized in Fig. 2 for a yz-plane $(x = a)$ perpendicular to the direction of propagation, with (yh, zh) being the origin. For this case, the source wave is travelling in the positive x-direction, and so the reference direction for polarization is the negative y-direction. It can be noted that a mutually perpendicular vector couplet of the electric and magnetic fields for a given point in space rotates through the angle ψ with the distance vector.

A standard FDTD code can thus be modified to implement this line source. It is a simple procedure to modify the standard plane wave source implementation to allow for such a case. In this case, the angle ψ is no longer fixed for all points on the Huygen's surface, but changes depending on the point location with respect to the line.

2.5. *Staircase Errors*

Approximation of smooth boundaries by cubic voxels associated with FDTD is well known to result in computational errors. There have been a number of reports on techniques

that employ mesh refinement in the context of FDTD methods. They can be roughly divided into four groups:

1. Mesh refinement techniques (e.g., subgridding and graded meshes);
2. Locally conformal meshes;
3. Subcell models; and
4. Finite volume techniques (FVTD).

The methods in the first group do not effectively address the issues because they simply increase the density of the mesh while retaining the underlying staircase approximation. Locally conformal meshes are successful for PEC boundaries. High frequency applications of such conformal meshes have been applied to dielectric interfaces, but they had a small effect on accuracy. Subcell modelling considers an effective dielectric constant for cells not aligned with cell boundaries based on weighted flux averaging through a cell face. Such techniques are again successful in high frequency applications of FDTD, but fail in the low-frequency as pointed out in [16]. Finally, the FVTD approach (or a hybrid method) can solve the staircase problem in question but this involves a different numerical technique which is beyond the scope of this paper.

Regardless of the refinement techniques available, the main staircasing error in the quasi-static method occurs where the conductivity gradient is highest—normally the air–conductor interface. Since we are interested mainly in the internal organ dosimetry, staircasing errors are not absolutely critical for these types of problems. As such, subcell averaging will suffice for the problem at hand.

3. METHOD VERIFICATION

3.1. *Fields in Free Space*

First the cylindrical TEM line-source implementation was validated by exciting an empty computational domain (free space) with the infinite line-source function. To model this situation, a domain of $20 \times 110 \times 110$ cm was utilized, with a grid resolution of 1 cm in each direction. The line source was oriented in the x-direction, centered 50 cm over the domain, i.e., $(yh, zh) = (55\text{ cm}, 155\text{ cm})$. The domain was terminated by a PML (6, P, 40dB) (six layers, with a parabolic profile, and with 40-dB attenuation for normal incidence) on all sides. The time excitation was the function given by Eq. (1). The simulation was run for 200 time steps to allow for the wave to fully traverse the domain. The fields at $N_{\Delta t} = 200$ were then compared with the analytic solution. As shown in Table I, the resultant fields are in excellent agreement globally with the analytic results. As expected, the Cartesian mesh representation of cylindrical fields introduces longitudinal fields that are nonphysical, but

TABLE I
Relative Errors in Electric Field for the Empty Domain

	Maximum		Average	
Grid resolution	Horizontal (y)	Vertical (z)	Horizontal (y)	Vertical (z)
Coarse (2 cm)	0.0910%	0.0188%	0.0078%	0.0022%
Fine (1 cm)	0.0114%	0.0036%	0.0018%	0.0005%

they are negligibly small, i.e., on the same order of magnitude as the error fields in the transverse directions.

3.2. *Conductive Sphere*

Recollecting that the motivation for this work is to investigate electric fields induced in humans at powerline frequencies by a line-source, it is relevant to model a simple object for which the problem has an analytic solution, e.g., a conductive sphere of a size comparable to the human body. The material parameters of the sphere are also chosen to represent nominal values in the human body.

In order to validate the FDTD method at low frequencies for the line source, both the electric field and the magnetic field exposures are investigated. Comparisons are made based on average, root mean square (RMS), and maximum induced electric fields in the sphere. The closed form solutions for fields induced in a homogeneous lossy sphere by an infinite current line (magnetic field) and an infinite line of charge (electric field) are reported in [14, 15]. The relative and absolute errors are also investigated to establish validity of the method and to identify locations of large errors.

For both electric and magnetic exposure the problem simulation was formulated as follows. A conductive sphere of similar size and conductivity to those of the human body (conductivity = 0.1 S/m, radius = 50 cm) was selected. With these parameters, at low frequencies, the conduction current is much greater than the displacement current, and the quasi-static approximations apply. The staircased sphere was centered in a computational domain of size 110 × 110 × 110 cm, terminated on all sides by a PML (9, P, 60 dB). From previous research [16], large errors are expected at the surface of the staircased sphere. Their magnitude depends on the shape of the staircasing and conductivity contrast. To partially mitigate these effects, subcell averaging of material parameters can be used in our FDTD program.

As previously, a standing wave was created for magnetic or electric field excitation with two waves of proper orientations traveling from the opposite directions on a line source. The line was assumed oriented in the x-direction, centered 50 cm over the sphere, i.e., $(yh, zh) = (55\text{ cm}, 155\text{ cm})$. Source function parameter values were chosen to simulate a 1 A (peak) current of 60 Hz in the magnetic field case. For the electric field case, source function parameters were chosen to simulate a field of 1000 V/m in the absence of the sphere at the center of the domain (1 m from the line); this corresponds to a line charge density of $\rho = 2000\pi\varepsilon_0$ C/m. Simulations were performed with a grid resolution of 1 cm. Steady state was reached after 2000 time steps.

3.2.1. Magnetic induction. Figures 3–5 show the individual calculated field components at representative cross-sections in the three directions, along with the corresponding analytic solution for comparison. It is apparent that the field spatial distributions are very similar, except in some cases (especially the E_z and E_y fields). The high field values in the numerical solution tend to obscure the visual representation of the actual field distribution. Figure 6 shows the total field ($E_{\text{tot}} = \sqrt{E_x^2 + E_y^2 + E_z^2}$) distribution throughout the sphere, which is in excellent agreement with the analytic solution. Point-by-point relative errors were examined, with the result that the locations of high relative error are concentrated at the surface of the sphere. There are large relative errors at the very center also that are associated with zero field value in the analytic solution. Thus a computed field there, however small, represents an infinitely large relative error.

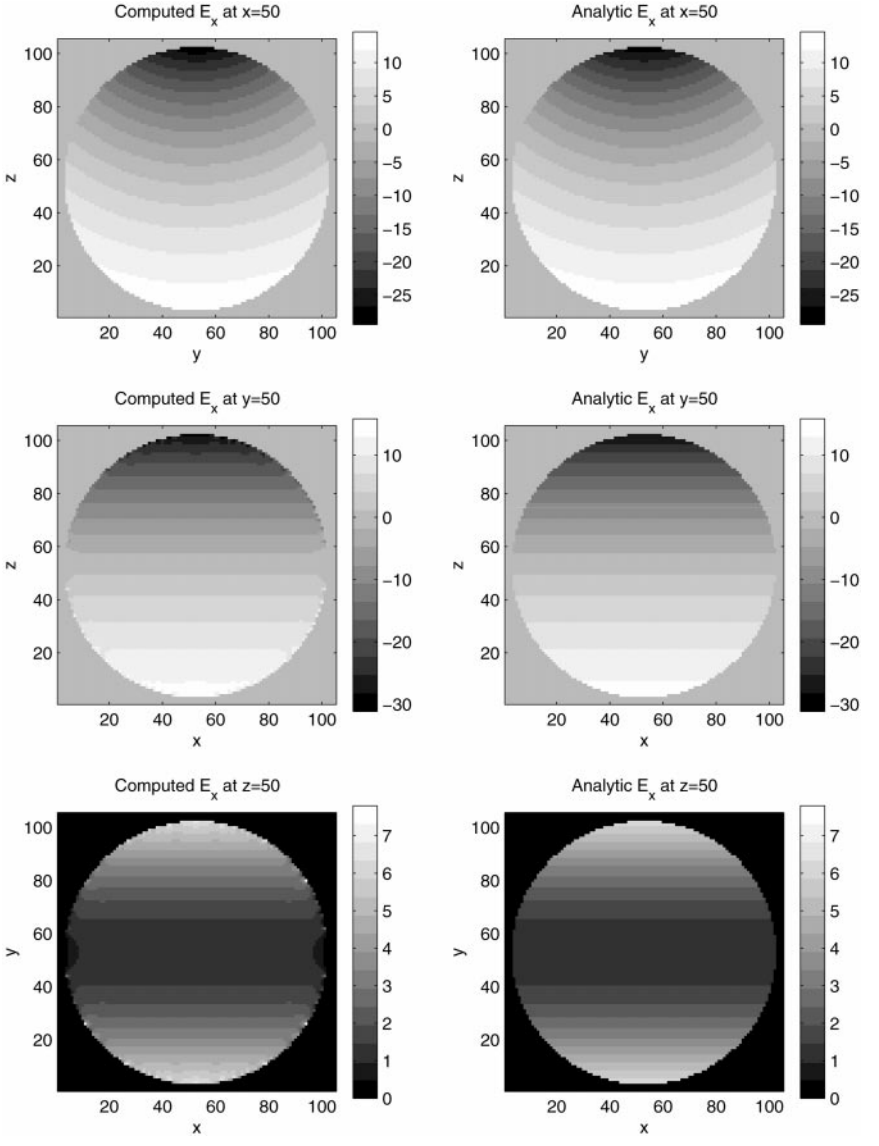

FIG. 3. Magnetic induction in a lossy sphere from a 60-Hz line source (1000 V/m at $r = 1$ m)—Induced E_x-field (in μV/m) for cross sections in the three principal planes (computed vs analytic).

Table II provides a more quantitative evaluation of the errors. The computed maximum field is much greater than the analytic maximum field. However, the average field is very close to the analytic average field, as is the RMS. Relative errors in the total fields are larger in the upper half of the sphere compared to the lower half and range around 25–30% on average at the surface of the sphere. Relative errors in the total fields at interior points are less than 0.5%, in general. The last row in the table represents the maximum error in the respective fields, computed point by point.

Combining the qualitative and quantitative results, the following observations can be made: the quasi-static FDTD method with the line source accurately models the induced field distribution and field values in the interior of lossy objects, but field values close to object boundaries are overpredicted by up to 33%.

TABLE II
Computed vs Analytic Results for Magnetic Induction—No Subcell Averaging

	Maximum	Average	RMS
Computed total electric field (μV/m)	37.778	11.142	12.162
Analytic total electric field (μV/m)	28.502	11.138	12.154
% Difference ($\lvert\frac{\text{computed-analytic}}{\text{analytic}}\rvert \times 100$)	33%	0.03%	0.07%
Error field (|computed-analytic|) (μV/m)	10.404	0.0811	0.377

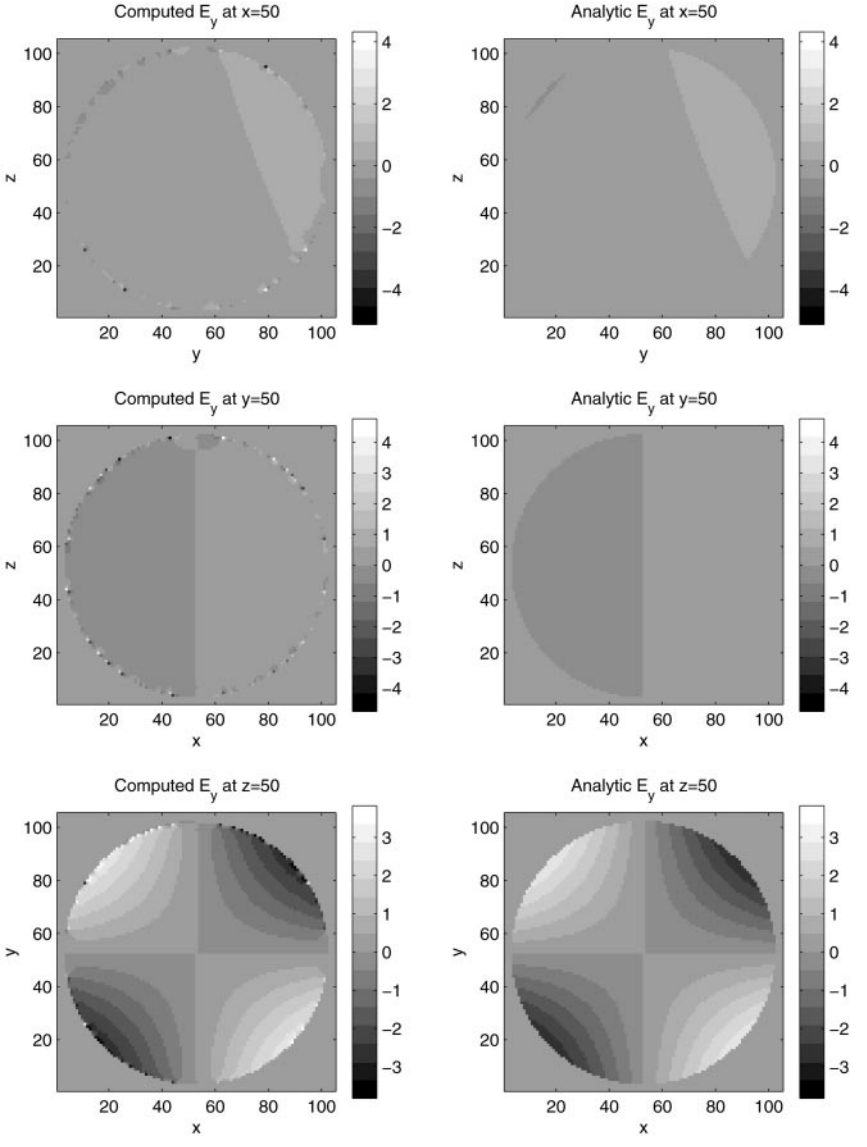

FIG. 4. Magnetic induction in a lossy sphere from a 60-Hz line source (1000 V/m at $r = 1$ m)—Induced E_y-field (in μV/m) for cross sections in the three principal planes (computed vs analytic).

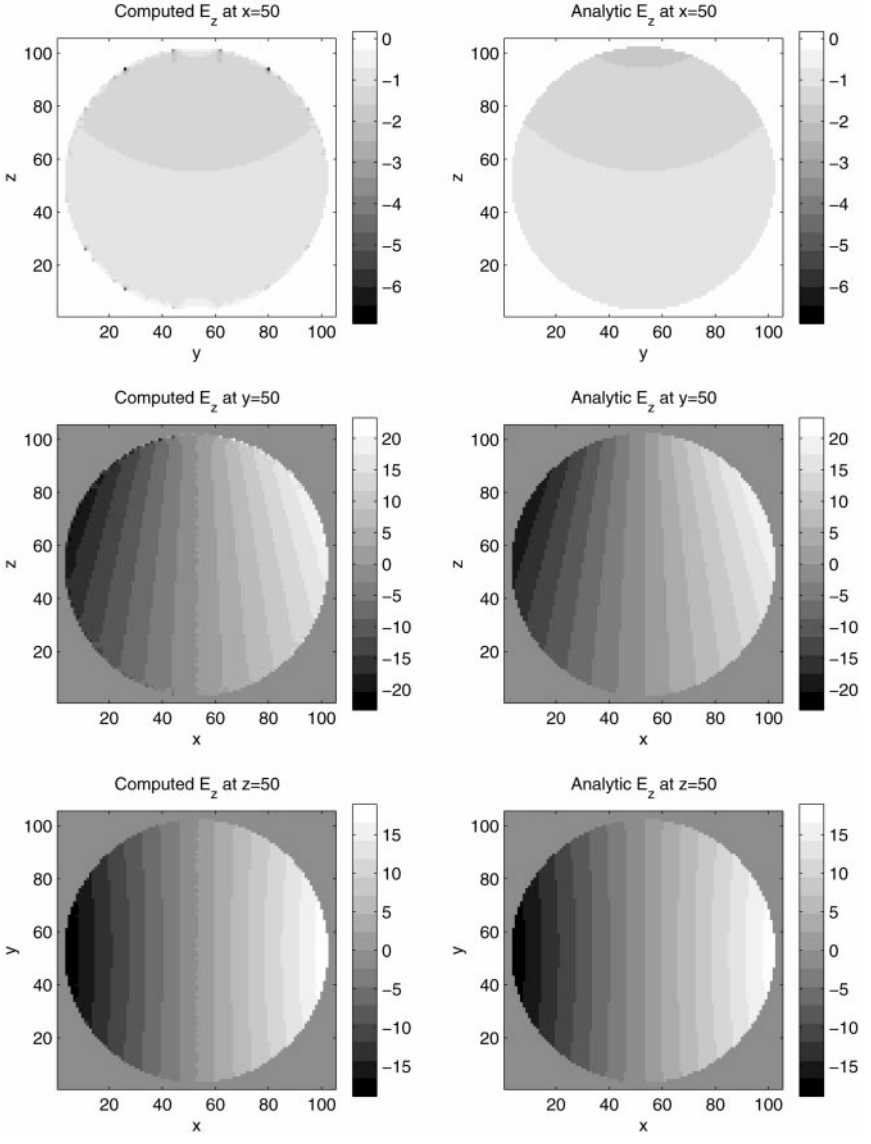

FIG. 5. Magnetic induction in a lossy sphere from a 60-Hz line source (1000 V/m at $r = 1$ m)—Induced E_z-field (in μV/m) for cross sections in the three principal planes (computed vs analytic).

The problem of large errors at the boundaries of the staircased sphere are a direct result of the staircasing, causing enforcement of the boundary conditions different from the original object, and the abrupt transition in material properties. This abrupt transition can be mitigated by the use of subcell averaging of material properties in the preprocessing stage of a FDTD simulation. Subcell averaging can best be understood by imagining an offset 2-dimensional grid near a particular field location, with that field location at the centre of its corresponding offset grid space. This offset grid is then subdivided into N equal sections. The material parameter assigned to the indexed field location is the weighted average of the material properties in the centre of each subdivision. In the case of the homogeneous sphere of interest, the effect is to create a layer at the boundary whose conductivity values range from 0 to 0.1 S/m.

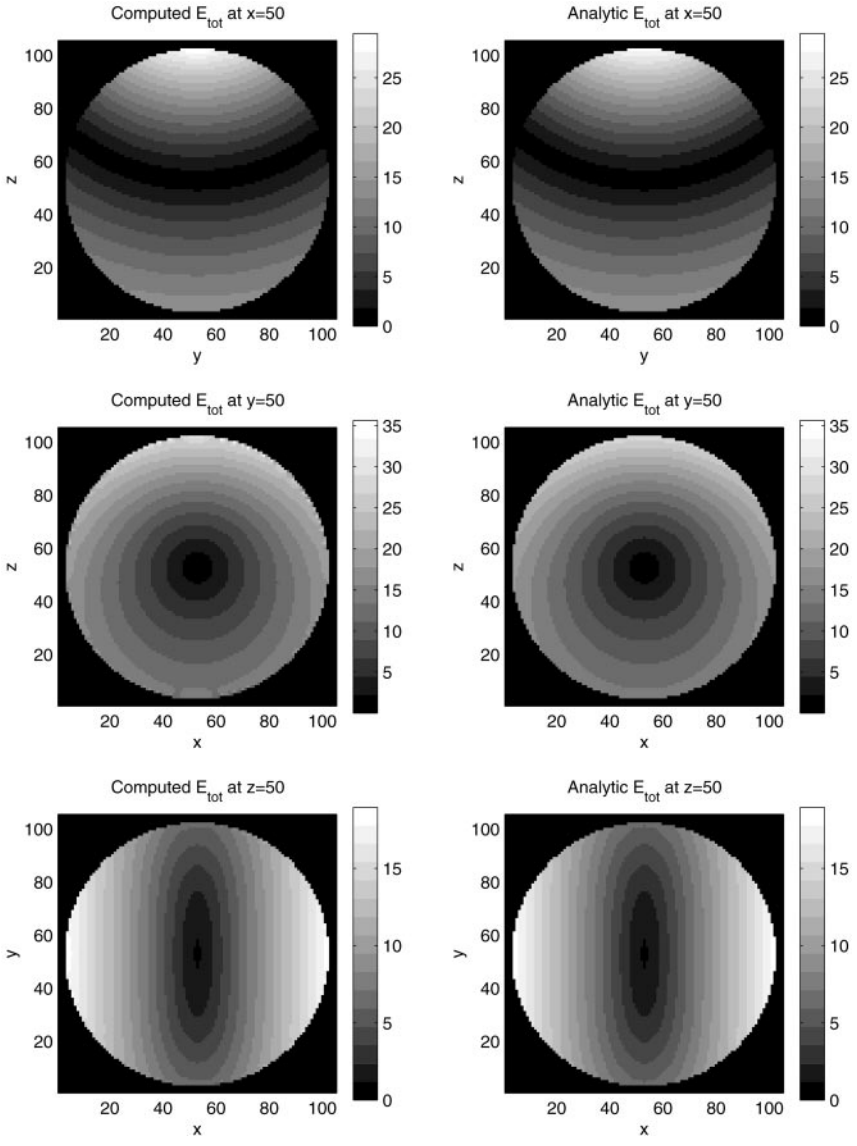

FIG. 6. Magnetic induction in a lossy sphere from a 60-Hz line source (1000 V/m at $r = 1$ m)—Induced E_{tot}-field (in μV/m) for cross sections in the three principal planes (computed vs analytic).

Table III provides the quantitative look at the errors with subcell averaging of $N = 2$ and $N = 8$. It is evident that the computed maximum field is larger than the analytic maximum field (18.7% with $N = 2$, 5.5% with $N = 8$), but less than that with no averaging. The average field is still very close to the analytic average field, as is the RMS. The absolute and relative errors have been reduced, meaning more accurate prediction of fields point by point. The relative errors are still larger in the upper half of the sphere compared to the lower half, but have reduced overall. For instance, on the sphere boundary the relative errors range from 15–25% on average.

The conclusion that can be made at this point is that simulations for magnetic induction using subcell averaging produce more accurate results and can significantly improve the

TABLE III
Computed vs Analytic Results for Magnetic Induction with Subcell Averaging

	Maximum		Average		RMS	
Subcell averaging	$N = 2$	$N = 8$	$N = 2$	$N = 8$	$N = 2$	$N = 8$
Computed total electric field (μV/m)	33.824	30.079	11.196	11.233	12.215	12.253
Analytic total electric field (μV/m)	28.502	28.502	11.188	11.222	12.205	12.241
% Difference ($\lvert\frac{\text{computed-analytic}}{\text{analytic}}\rvert \times 100$)	18.7%	5.5%	0.07%	0.1%	0.08%	0.1%
Error field (|computed-analytic|) (μV/m)	8.689	3.131	0.0426	0.0109	0.195	0.0650

determination of maximum field values with higher levels of subcell averaging. Field values at object boundaries are still overpredicted, but the error in these fields can be greatly reduced.

3.2.2. Electric induction. The results for electric induction in the sphere are shown qualitatively in Figs. 7–9. No figure is presented for the E_x field, as the analytic solution is zero everywhere. As is the case for magnetic induction, there are very large field values on the surface of the sphere, but the errors are greater than for the magnetic field induction. The field distributions are still matching to the analytic field configurations. Relative errors are still highly concentrated on the surface of the sphere.

Table IV provides quantitative results. The computed maximum field is much greater than the analytic maximum field. In this instance the location of maximum absolute error is actually the location of maximum relative error and exists around the entire boundary of the topmost part of the staircased sphere. That is the location of the maximum source field as well. However, the average field is very close to the analytic average field, as is the RMS, though the large errors in maximum values introduce larger errors in the RMS.

These results indicate that the FDTD method is not satisfactory at predicting maximum induced fields, but is still valuable for predicting field distributions and average field values. Previous research with plane wave sources has indicated that the method is still valuable because the conductivity gradients in the interior of the human body model are not as great as in the case considered here, in which the conductivity of free space is zero, representing an infinite conductivity gradient at air–tissue interfaces [16]. No simulations were performed with subcell averaging in the case of electric induction, as previous research showed that the averaging actually increased the errors [16].

The large errors evident in electric field induction are mostly a result of the staircasing approximation of smooth surfaces (this is elaborated in the following section). The

TABLE IV
Computed vs Analytic Results for Electric Induction—No Post-Processing

	Maximum	Average	RMS
Computed total electric field (μV/m)	489.21	103.23	105.46
Analytic total electric field (μV/m)	178.27	102.26	104.28
% Difference ($\lvert\frac{\text{computed-analytic}}{\text{analytic}}\rvert \times 100$)	174.4%	0.9%	1.1%
Error field (|Computed-analytic|) (μV/m)	310.93	1.542	5.639

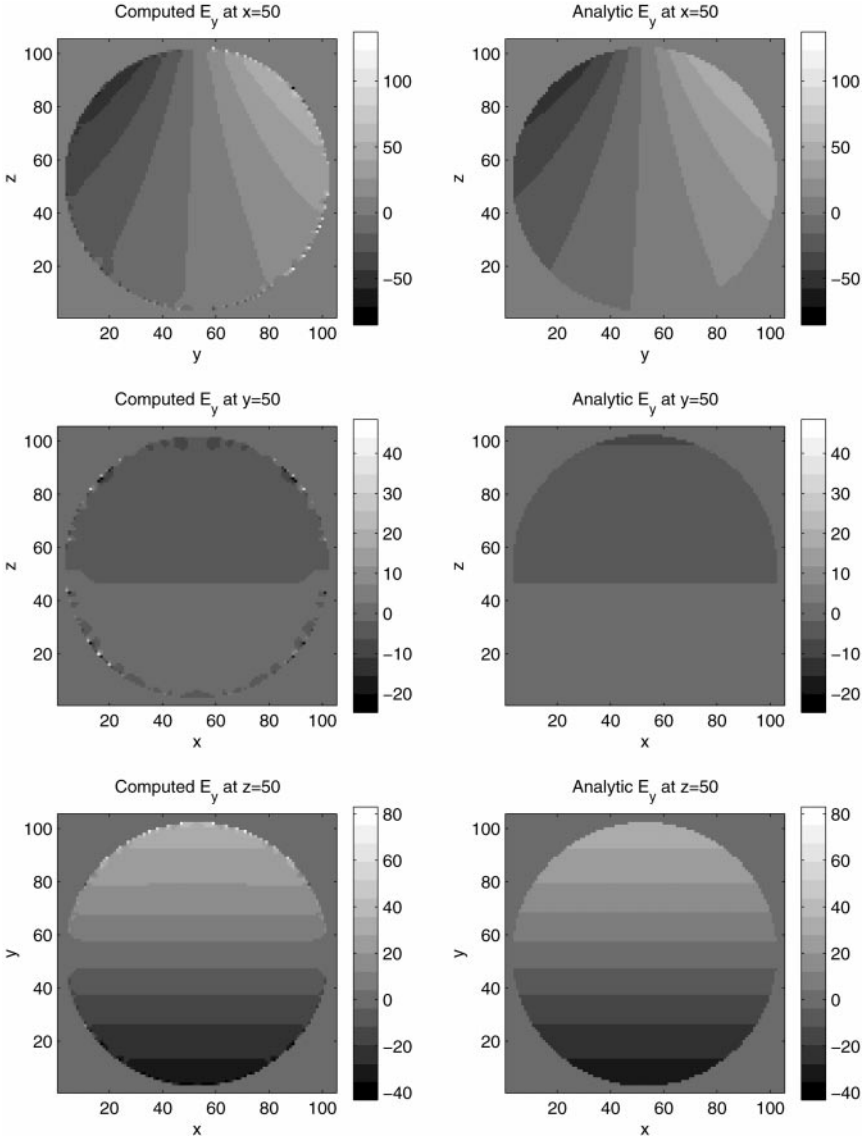

FIG. 7. Electric induction in a lossy sphere from a 60-Hz line source (1000 V/m at $r = 1$ m)—Induced E_y-field (in μV/m) for cross sections in the three principal planes (computed vs analytic).

immediate cause is the strict enforcement of boundary conditions. This may also be used as a solution, given that the problem of interest represents a very good conductor in quasi-static conditions. It is then reasonable to let tangential electric fields at the boundary be zero (i.e., the limit for a perfect conductor). This is easily implemented in the postprocessing of the data. The external boundary tangential electric field components are identified and set to zero. As a result, the erroneously large computed fields are corrected, and hence the accuracy of the prediction is improved for both the maximum and the average electric fields induced.

Table V shows the results using postprocessing of the previous data for two different grid resolutions. The postprocessing has reduced the maximum error significantly, and the

TABLE V
Computed vs Analytic Results for Electric Induction—Surface Tangents Set to Zero

	Maximum		Average		RMS	
Grid resolution	1 cm	2 cm	1 cm	2 cm	1 cm	2 cm
Computed total electric field (μV/m)	224.18	385.45	98.68	104.22	102.50	106.62
Analytic total electric field (μV/m)	178.27	176.79	97.93	102.51	101.77	104.51
% Difference ($\lvert\frac{\text{computed-analytic}}{\text{analytic}}\rvert \times 100$)	25.8%	118%	0.8%	1.67%	0.7%	2.02%
Error field (|computed-analytic|) (μV/m)	68.12	208.99	1.042	2.679	2.023	7.714

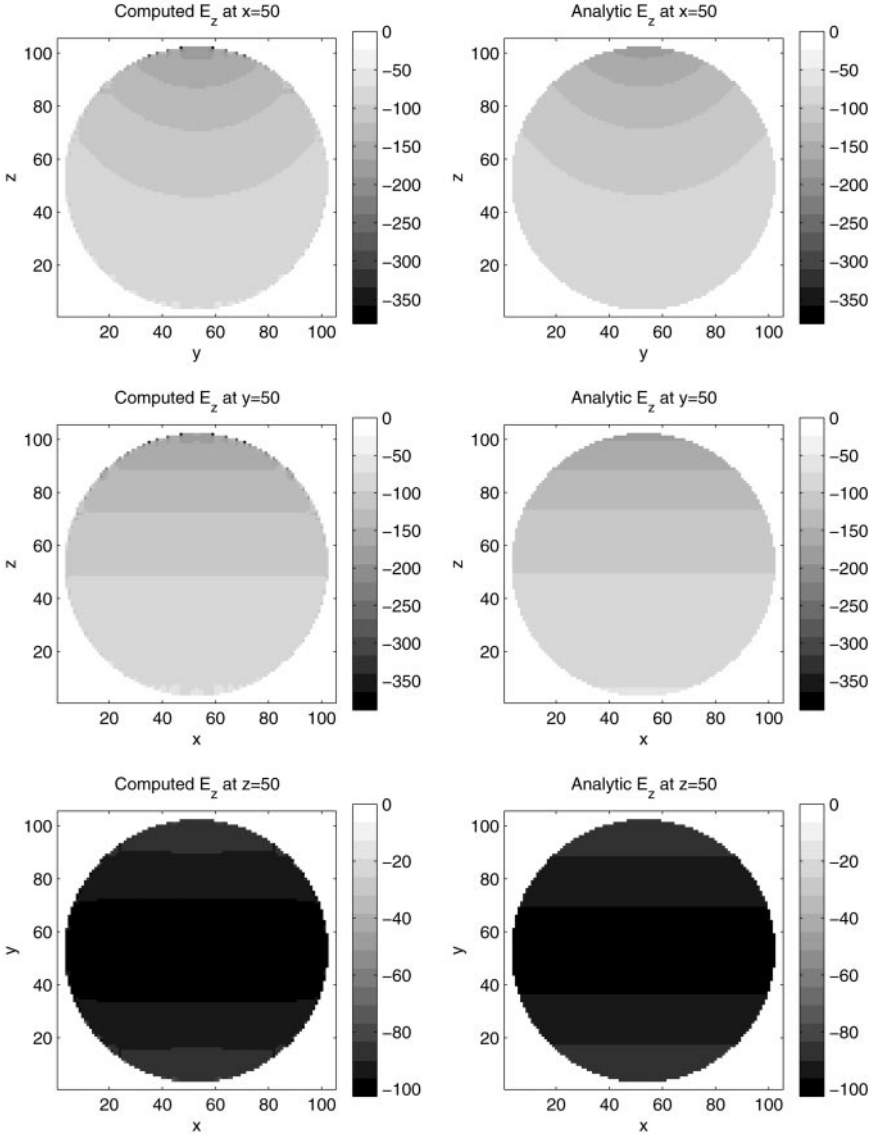

FIG. 8. Electric induction in a lossy sphere from a 60-Hz line source (1000 V/m at $r = 1$ m)—Induced E_z-field (in μV/m) for cross sections in the three principal planes (computed vs analytic).

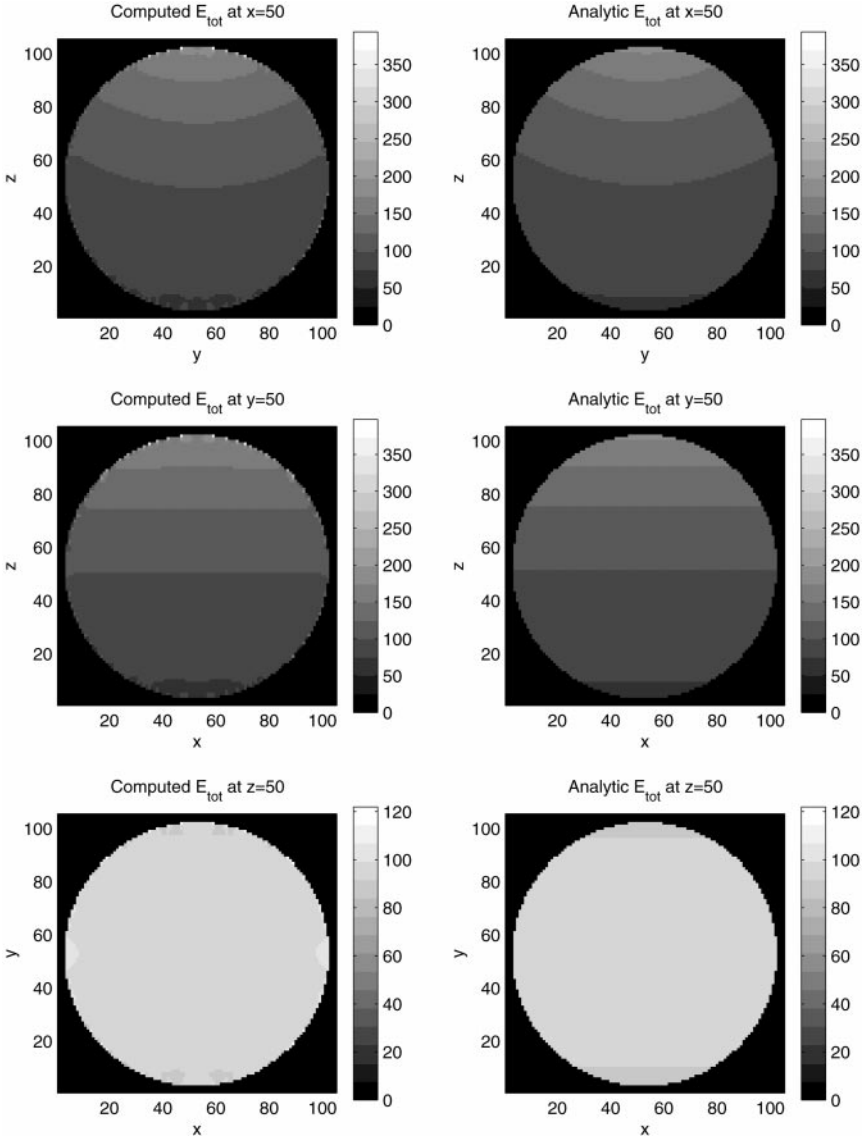

FIG. 9. Electric induction in a lossy sphere from a 60-Hz line source (1000 V/m at $r = 1$ m)—Induced E_{tot}-field (in μV/m) for cross sections in the three principal planes (computed vs analytic).

average and RMS errors as well. Computed maximum fields are still overpredicted. It is expected that by using a finer grid the errors can be further reduced. Since our computer resources do not allow us to use a finer grid, we used a coarser grid of 2 cm to illustrate the effect of the grid size. As expected, the errors increase for this coarser resolution.

3.2.3. Explanation of sources of error. Any staircasing approximation changes the object's actual shape and thus the discretized Maxwell's equations enforce different fields at the boundaries than for the actual object. The effects are noticed principally at locations where there is a large discontinuity in material properties. In the FDTD, it is particularly noticeable for the electric field, as the electric field components are always located on voxel edges, where the object material properties change. Considering a sphere as an example, it

is known that the tangential electric field must be continuous across the boundary, and the normal electric flux density must be continuous. By introducing a staircase, we also force continuity conditions which must adapt to abrupt changes in surface normal direction, hence disrupting the expected distribution of fields; what is actually simulated is a building block representation of the object.

For magnetic induction the staircasing forces induced currents to flow a path different from that in a real sphere. High current density is artificially introduced in inner corners of some voxels, resulting in higher than expected field values. For a sphere, the induced currents near the surface would flow continuously around the smooth contour of the sphere. But in the staircased sphere, currents near the surface are impeded by the step approximations. Current flow is effectively constricted around inside corners, resulting in high current density (overpredicted values). This is much like the flow of water near a right angle wedge that lies in its path.

For electric induction, first consider that a very good, albeit imperfect, conductor is simulated. As is known for conductors illuminated by incident electric fields, the induced currents and charges tend to concentrate at sharp edges or corners, creating field singularities. Although the sphere is smooth (and hence would show no charge singularities), simulations actually model a staircased sphere which consists of multiple sharp corners. The results from these simulations show that fields are highly overpredicted, as the program tries to accurately reflect the true singularities that are expected at corners of a staircased object.

The errors in this work are of similar character and magnitude to those encountered for plane wave excitation [16]. This has implications for any simulations involving studies of more complicated lossy structures, since maximum field values for isolated volumetric regions will be overpredicted if the region contains boundaries with high conductivity gradients.

4. FIELD INDUCED IN THE HUMAN BODY

The quasi-static FDTD method with a line-source can be used to compute induced electric fields and currents in the human body close to transmission lines, where the incident electric field can no longer be considered uniform. A heterogeneous model of the human body is based on MRI scans and has been developed from a head and torso model from [17] with skin and limbs added in our laboratory. The original resolution of the model was 3.6 mm, but for this research it was reduced to 7.2 mm by assigning to each coarse voxel the tissue type most prevalent in the vicinity of the fine-scale model. In all computations the z-axis of the coordinate system is from foot to head (vertical), the x-axis is from left to right, and the y-axis is from back to front. The various organs and tissues were assigned conductivity ranging from 0.01 to 2.2 S/m, based on the most recent measurements. Detailed conductivity values are given in [18]. Because the displacement current is negligible, relative permittivity values were set to 1 for all material types to avoid relaxation effects.

4.1. *Geometry of the Problem*

The body model and the bounding box encompassing it were placed in contact with a perfect ground plane. The remaining five sides were surrounded by four layers of free space cells and PMLs (15, P, 40dB). This led to an overall computational domain of $114 \times 83 \times 264 = 2{,}497{,}968$ voxels. In order to initiate the proper analytic fields in the computational

domains, four line-source functions had to be initiated: two for each of the real and image source (as a result of the ground plane). As noted previously, two sources created the standing wave condition for the electric field excitation. The source functions simulated source (image) lines located 4 m above (below) the ground plane, oriented parallel to the x-axis, and centred over the domain. The parameters of the functions were chosen to represent a 60-Hz field, with a magnitude of 1 kV/m at the ground plane directly underneath the line. All results presented scale linearly with amplitude and with frequency up to 100 kHz [5].

4.2. *Results and Discussion*

Steady state for this object was reached after 8000 time steps. The induced electric fields at the end of the simulation were the data of interest and were analyzed as follows. First, organ dosimetry data in terms of the induced electric field and current density maximums and averages for organs of interest were determined and compared with comprehensive organ dosimetry obtained previously in the case of a uniform 1-kV/m field. Most of the organs chosen were those whose ratio of surface area to volume were suitable for analysis, given that boundary field values are overestimated and may skew data. None of the data was postprocessed in the manner discussed above (setting tangential surface fields to zero), since it is the internal organs that are of interest. The results are shown in Table VI. The uniform field used for comparison is 1 kV/m. All the values for the line source are higher, by up to 40%, as is expected since the fields in the absence of the object are higher than those of a uniform field.

It is informative to compare the ratio of the induced fields with the line source to that of the uniform field and relate that to the fields that exist in the absence of the body for each source, respectively. This is done in the following manner. For a particular organ a suitable coordinate location P is identified as an approximate centre of the organ. Then the ratio

TABLE VI
Organ Dosimetry for Electric Induction from 60-Hz Line Source at 4 m over a Perfect Ground Plane

	$\|E\|_{max}$ (mV/m)		$\|J\|_{max}$ (mA/m)		$\|E\|_{avg}$ (mV/m)		$\|J\|_{avg}$ (mA/m)	
Organ	Line source	Uniform	Line source	Uniform	Line source	Uniform	Line source	Uniform
Bowels	3.74	3.20	1.27	1.36	1.18	0.946	0.374	0.305
Brain	4.45	2.82	0.445	0.282	1.21	0.869	0.101	0.0727
Brain—gray	4.45	2.82	0.445	0.282	1.14	0.828	0.114	0.0828
Brain—white	2.80	2.22	0.168	0.133	1.32	0.940	0.0790	0.0564
Heart	3.18	2.19	0.318	0.219	1.49	1.07	0.149	0.107
Kidneys	2.75	2.43	0.275	0.242	1.38	1.03	0.138	0.103
Liver	4.07	2.69	0.285	0.188	1.76	1.26	0.123	0.0884
Lungs	3.23	2.30	0.259	0.184	1.36	1.01	0.108	0.0805
Muscle	27.6	23.5	9.65	8.21	1.47	1.32	0.515	0.462
Prostate	2.23	2.26	0.893	0.904	1.49	1.47	0.596	0.589
Spinal cord	3.55	2.23	0.355	0.223	1.29	1.08	0.129	0.108
Spleen	3.48	2.29	0.348	0.229	1.74	1.36	0.174	0.136
Stomach	1.63	1.33	0.815	0.666	0.854	0.684	0.427	0.342
Thyroid	1.14	0.962	0.572	0.481	0.911	0.819	0.456	0.410
Whole body	75.2	48.1	12.01	11.5	2.031	1.70	0.349	0.309

TABLE VII
Ratios of Electric Fields induced by a Line Source to Those of a Plane Wave, along with the Free-Space Ratio R_p

Organ	R_P	OR_a	OR_m
Bowels	1.084	1.249	1.169
Brain	1.218	1.389	1.578
Brain—gray matter	1.218	1.380	1.578
Brain—white matter	1.218	1.401	1.263
Heart	1.125	1.391	1.451
Kidneys	1.097	1.344	1.130
Liver	1.106	1.398	1.511
Lungs	1.131	1.343	1.405
Spleen	1.105	1.280	1.517
Stomach	1.106	1.334	1.225

(R_P) of the field at that location in the absence of the body model to that of the uniform field strength of 1 kV/m is computed. Next the organ maximum and average induced electric field values for the line-source exposure and the uniform field exposure are compared, and two other ratios OR_a and OR_m are constructed, representing the ratios for the organ average and maximum values. Finally, these organ ratios are compared to the exposure field ratio R_P. The steps are thus as follows:

1. determine a midpoint, P;
2. at P, find the free-space field for the line-source $E_l(P)$;
3. determine the free-space ratio $R_P = (E_l(P))/1000$ V/m;
4. determine organ ratios for maximum and average induced electric fields OR_m and OR_a; and
5. compare organ ratios with free-space ratios R_P.

The results of this process are tabulated in Table VII. This process is informative because the results obviously show that the induced field ratios are much larger than the free space ratio at the position of every organ of interest. Where the free space ratio R_P ranges from 108–120%, the organ ratios for both the average and the maximum induced fields are higher, ranging from 116–160%.

Another calculation of interest is the total vertical current through each layer of the model. This data is illustrated in Fig. 10, along with the corresponding vertical current previously calculated for a uniform field of 1000 V/m. It is readily evident that the vertical current predicted by exposure to the line source is slightly greater than that for the uniform field, as is expected since the field at the head from the line source is approximately 20% higher than that of the uniform field.

Finally it is useful to examine the maximum external electric field, or more importantly the field enhancement factor. The field enhancement factor is a ratio of the external field in the presence of the body to that in the absence of the body. The enhancement factor predicted for the case of a uniform field is 16.8 [10]. In the present research for exposure to a line source, the predicted enhancement factor is 19.0. It should be noted that the maximum external field is likely to be overpredicted because of the staircasing approximation. Indeed, visual inspection of the vertical layer where the maximum field occurs (at the top of the head) shows a corona of high field values around the exterior, where a staircase edge occurs.

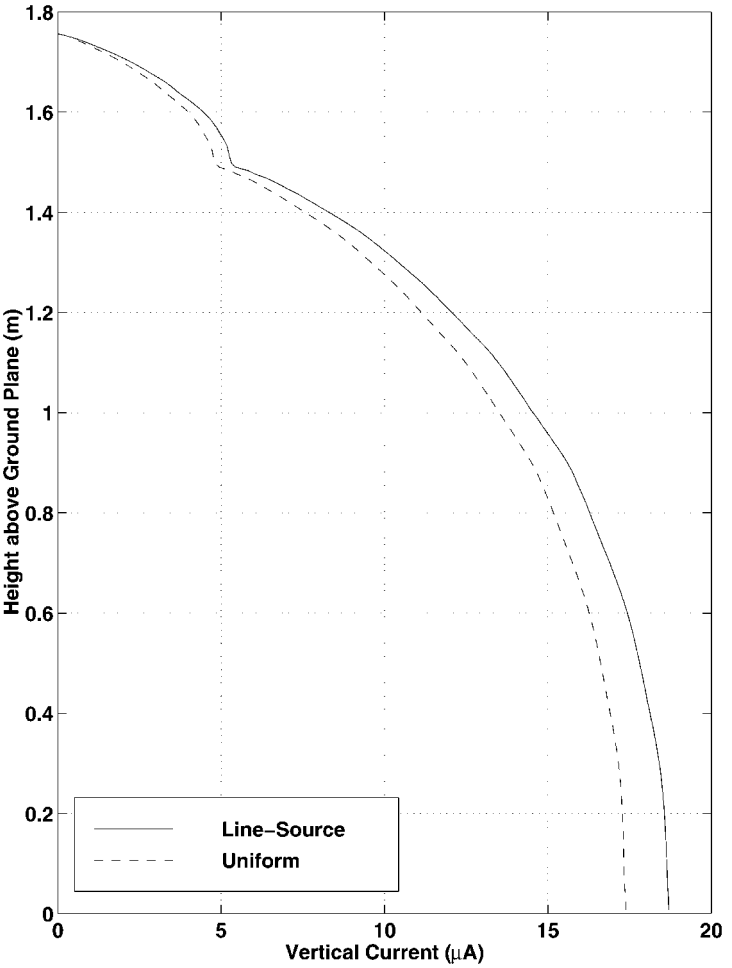

FIG. 10. Total vertical current (as a function of height) of the human model on a ground plane, in an electric field produced by a 60-Hz line source (1 kV/m at the ground).

But this error is consistent with and evident in the previous uniform field research as well, since the same staircasing approximation is used.

5. CONCLUSIONS

An extension to the total–scattered field formulation of wave excitation in the FDTD has been provided for line sources with TEM waves. The formulation based on the analytic formulation of the incident field is rather straightforward and is of high accuracy even for a coarse mesh. This formulation has been used in the recently developed quasi-static FDTD method. A verification of the method against an analytic solution for a conductive sphere in the proximity of a line source attests to its high accuracy. Finally, the combination of the new nonuniform source formulation and the quasi-static FDTD provides an effective tool for computations of induced electric fields and currents in the human body in close proximity to high voltage transmission lines. Such situations occur in some locations in the electric utility industries, and accurate evaluation of fields in the body is of importance, particularly for persons with medical devices, e.g., cardiac pacemakers.

ACKNOWLEDGMENT

The authors are grateful to Dr. T. W. Dawson for providing his computer code for computations of analytic results reported here. This work was supported by the Natural Sciences and Engineering Research Council of Canada (NSERC), BC Hydro, and the TransAlta Industrial Research Chair.

REFERENCES

1. E. Sonnendrücker, J. J. Ambrosiano, S. T. Brandon, A finite element formulation of the Darwin PIC model for use on unstructured grids, *J. Comput. Phys.* **121**, 281 (1995).
2. J. Van Bladel, *Electromagnetic Fields* (Hemisphere, New York, 1985).
3. K. S. Yee, Numerical solutions to initial boundary value problem involving Maxwell's equations in isotropic media, *IEEE Trans. Antennas Propag.* **14**, 302 (1966).
4. A. Taflove, *Computational Electrodynamics: The Finite Difference Time Domain Method* (Artech House, Norwood, MA, 1995).
5. J. DeMoerloose, T. W. Dawson, and M. A. Stuchly, Applicationi of the finite difference time domain algorithm to quasi-static field analysis, *Radio Sci.* **32**, 329 (1997).
6. J. P. Berenger, A perfectly matched layer for the absorption of electromagnetic waves, *J. Comput. Phys.* **114**, 185 (1994).
7. J. DeMoerloose and M. A. Stuchly, Reflection analysis of PML ABC's for low-frequency applications, *IEEE MGWL* **6**(4), 177 (1996).
8. J. P. Berenger, An effective PML for absorption of evanescent waves in waveguides, *IEEE MGWL* **8**(5), 188 (1998).
9. S. Gedney, An anisotropic PML absorbing media for the FDTD simulation of fields in lossy anisotropic media, *Electromagnetics* **16**, 399 (1996).
10. T. W. Dawson, J. DeMoerloose, and M. A. Stuchly, Hybrid finite-difference method for high-resolution modeling of low-frequency electric induction in humans, *J. Comput. Phys.* **136**, 640 (1997).
11. M. E. Potter, M. Okoniewski, and M. A. Stuchly, Extension of the FDTD method to non-uniform excitations, *Elec. Lett.* **34**, 2216 (1998).
12. T. W. Dawson and M. A. Stuchly, High resolution organ dosimetry for human exposure to low frequency magnetic fields, *IEEE Trans. Magn.* **34**, 708.
13. J. Stratton, *Electromagnetic Theory* (McGraw-Hill, New York/London, 1941).
14. T. W. Dawson, Low-frequency induction in a homogeneous sphere by line-sources Part I, Formulation and line current excitation, *Radio Sci.* (2000), in press.
15. T. W. Dawson, Low-frequency induction in a homogeneous sphere by line-sources Part II, Line charge excitation and discussion, *Radio Sci.* (2000), in press.
16. EPRI, *Validation of Computational Methods for Evaluation of Electric Fields and Currents Induced in Humans Exposed to Electric and Magnetic Fields*, Electric Power Research Institute (EPRI) Report TR-111768 (EPRI, Palo Alto CA, 1998).
17. I. G. Zubal, C. R. Harrell, E. O. Smith, Z. Rattner, G. R. Gindi, and P. H. Hoffer, Computerized three-dimensional segmented human anatomy, *Phys. Med. Biol.* **21**, 299 (1994).
18. R. L. S. Gabriel and C. Gabriel, The dielectric properties of biological tissues: III. Parametric models for the dielectric spectrum of tissues, *Phys. Med. Biol.* **41**, 2271 (1996).